Solid state detectors

Si, Ge
+ good energy resolution,
~0.1 %
- slow
- low stopping power

Scintillators

- bad energy resolution,
~ 6 % as best
+ fast – slow
+ high – low stopping power

---

wide bandgap semiconductors

CdTe, CdZnTe, HgI_2
+ high stopping power
- energy resolution ~ 1 %

new materials

+ high light yield
+ energy resolution ~ 3 %

	E_{gap} [eV]	$E_{e\text{-}h}$ [eV]
Si	1.12	3.61
Ge	0.74	2.98
CdTe	1.47	4.43
HgI_2	2.13	4.2
NaI(Tl)	5.9	15.3
CsI(Tl)	6.5	15.2

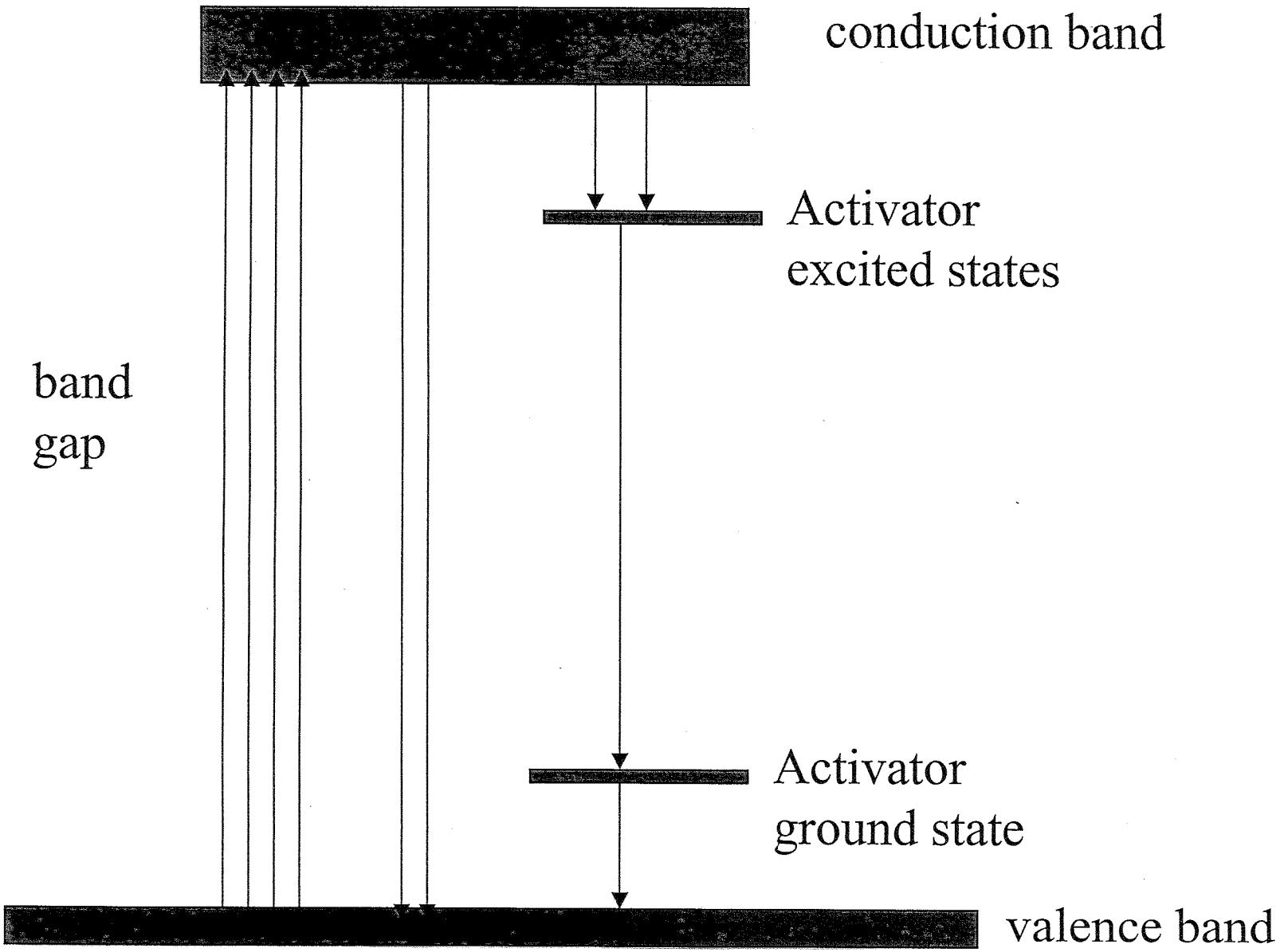
conduction band
Activator
excited states
band
gap
Activator
ground state
valence band

Inorganic scintillators

Scintillation photons are emitted from the activator excited states, fast transition, visible light.

Competing processes:
Electron arrives to excited states from which transition to ground state is forbidden. Additional small energy is required to lift the electron to other excited states (thermal excitation) with higher transition probability. This results in *phosphorescence radiation* radiation, or *"afterglow",* which is a slow time component.

Some excited states cause radiationless transitions, which represents loss mechanism in the conversion of the radiation energy to scintillation light. This is the *quenching effect.*

	τ [ns]	**λ_{max} [nm]**	**light yield [photons/MeV]**
NaI(Tl)	230	415	44 000
CsI(Tl)	1000	550	60 000
BaF_2	0.6/630	220/310	2200/7000
BGO $Bi_4Ge_3O_{12}$	300	480	8000

Scintillation process

- conversion to e-h pairs
- transfer to luminescence centre
- luminescence, i.e. photon emission

Number of emitted scintillation photons N_{ph} following absorption of gamma energy E_γ

$$N_{ph} = \frac{E_\gamma}{\beta E_{gap}} SQ$$

$E_{e-h} = \beta E_{gap}$ - energy required to produce one e-h pair

$\beta \sim$ 2-3 (mostly 2.3)

S – transfer efficiency of the e-h pair to luminescence centre

Q – efficiency for photon emission of the luminescence centre

	Energy gap (eV)
NaI (Tl)	5.9
CsI(Tl)	6.4
BaF_2	
fast	18.0
slow	10.6
ZnSe (Te)	2.6

Energy required to produce one e-h pair

$E_{e\text{-}h}=\beta E_{gap}$ $\beta\approx 2.3$ (2-3)

CsI (Tl) assume $E_\gamma = 1$ MeV

No. of light photons

1 MeV / 2.3 x E_{gap}=1 000 000 eV / 2.3x6.4≈67 000 photons

compare with measured 60 000 photons

For other crystals

E_γ=1 MeV

NaI (Tl)

1 000 000 eV / 2.3x5.9 eV ≈73 000 photons
measured 40 000 photons

BaF_2

fast 1 MeV / 2.3x18.0 eV≈24 000 photons
measured 1600 photons

slow 1 MeV / 2.3x10.6 eV ≈41 000 photons
measured 8000 photons

Radiative decay time for electric dipole emission

$\tau_r \sim \lambda^2$

more detailed

$$\tau_r = 1.5 \times 10^{-5} \quad \frac{\lambda^2}{f^{1/9}\left(n^2+1\right)^2 n}$$

f - oscillator strength of the transition

n - refractive index

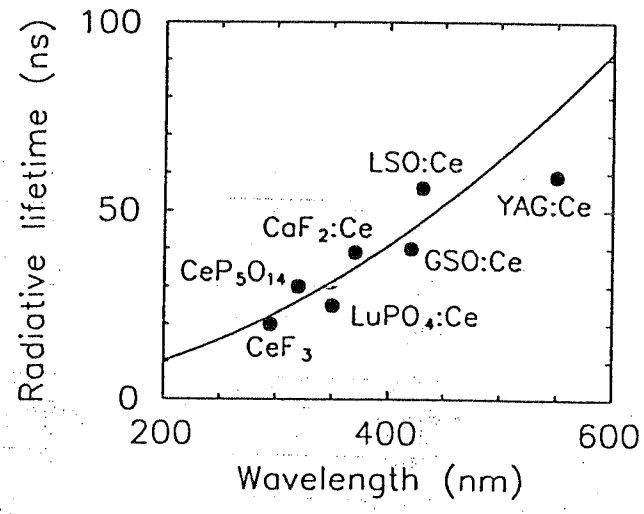

Fig. 2. The radiative lifetime vs wavelength. The oscillator strength, f, and refractive index, n, were taken equal to 0.0013 and 1.7, respectively. The points correspond to Ce d–f emission in different materials, as indicated. The decay times and emission wavelengths were taken: for GSO : Ce–$Gd_2(SiO_4)O$: Ce from [28], for LSO : Ce–$Lu_2(SiO_4)O$: Ce from [28], for YAG : Ce–$Y_3Al_5O_{12}$: Ce from [29], for CaF_2 : Ce from [29], for CeF_3 from [3,6], for CeP_5O_{14} from [4].

High light yield → low energy gap crystals → long wavelength of the scintillation light

Fast crystals → short λ (UV region) → high energy gap

Energy resolution

$$\left(\Delta E/E\right)^2 = \left(\delta_{sc}\right)^2 + \left(\delta_{st}\right)^2 + \left(\delta_n\right)^2$$

δ_{sc} – intrinsic resolution of the crystal

δ_{st} – statistical contribution

δ_n – dark noise contribution

For PM-tubes

$$\delta_{st} = 2.35x\left(1/N\right)^{1/2} x\left(1+\varepsilon\right)^{1/2}$$

N – number of photoelectrons
ε – variance of the electron multiplier gain

For avalanche photodiodes (APD)

$$\delta_{st} = 2.355x\left(F/N_{e-h}\right)^{1/2}$$

$N_{e\text{-}h}$ – number of e-h pairs
F – excess noise factor, reflecting the statistical fluctuation of the APD gain

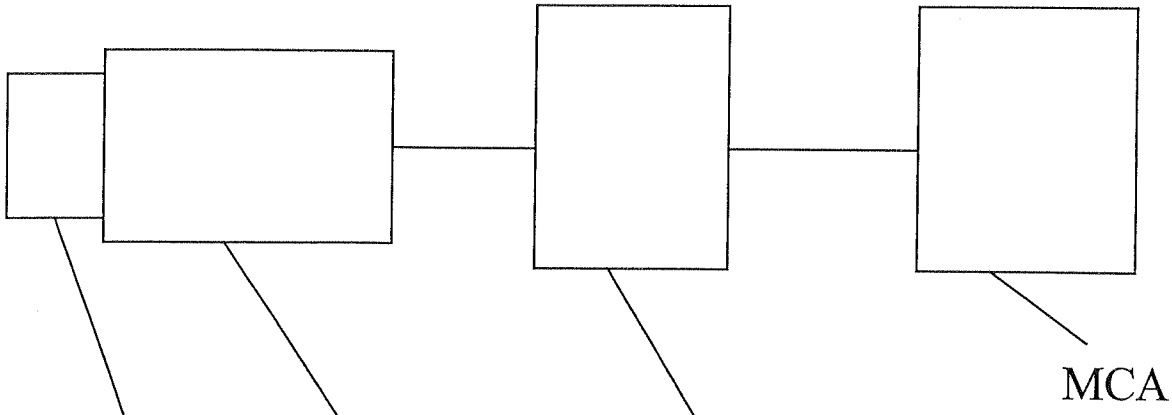

scintillator

photodetector:

PIN photodiode
PM-tube
avalanche photodiode

amplifier

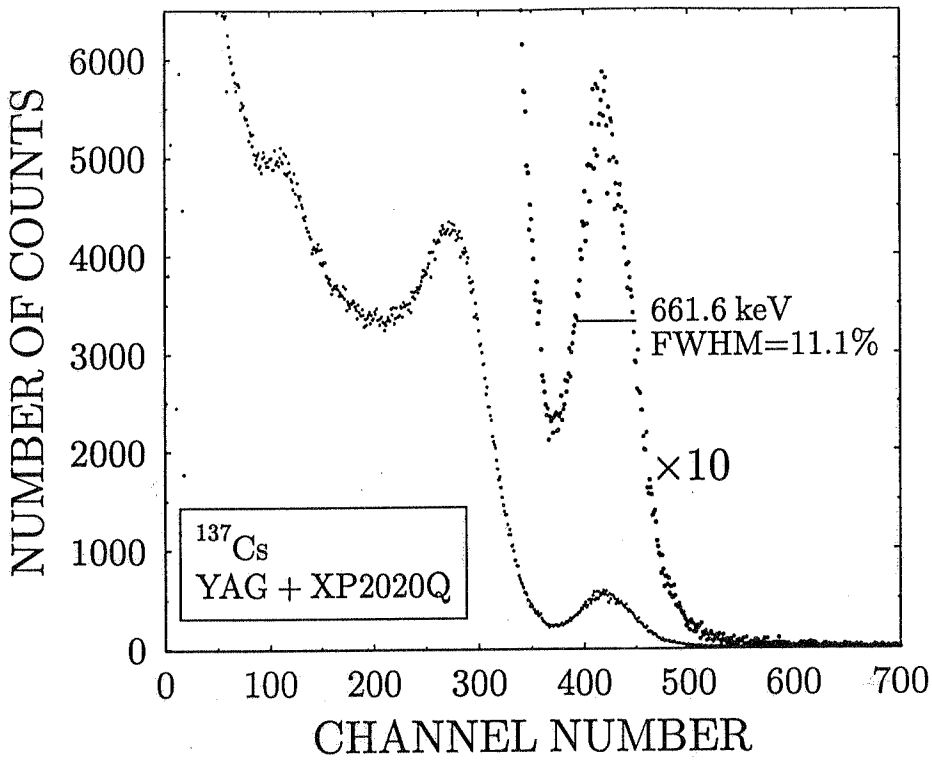
NUMBER OF COUNTS
6000
5000
4000
3000
2000
1000
0
0
100
200
300
400
500
600
700
CHANNEL NUMBER
661.6 keV
FWHM=11.1%
×10
137Cs
YAG + XP2020Q

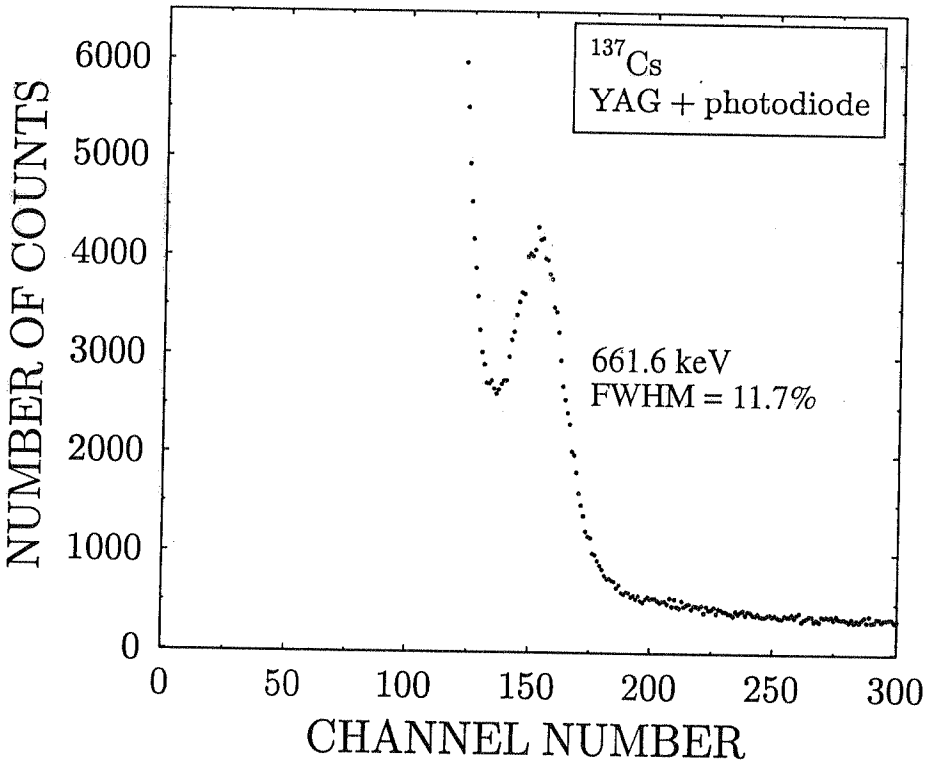
NUMBER OF COUNTS
6000
5000
4000
3000
2000
1000
0
0
50
100
150
200
250
300
CHANNEL NUMBER
137Cs
YAG + photodiode
661.6 keV
FWHM = 11.7%

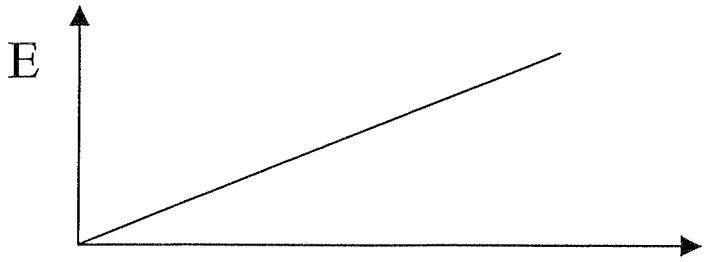

Channel no.

(light yield)

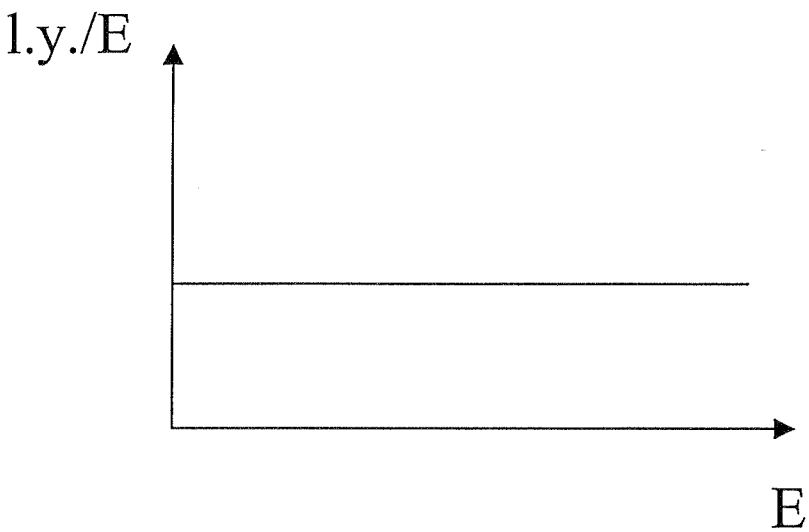

Light yield non proportionality in scintillators

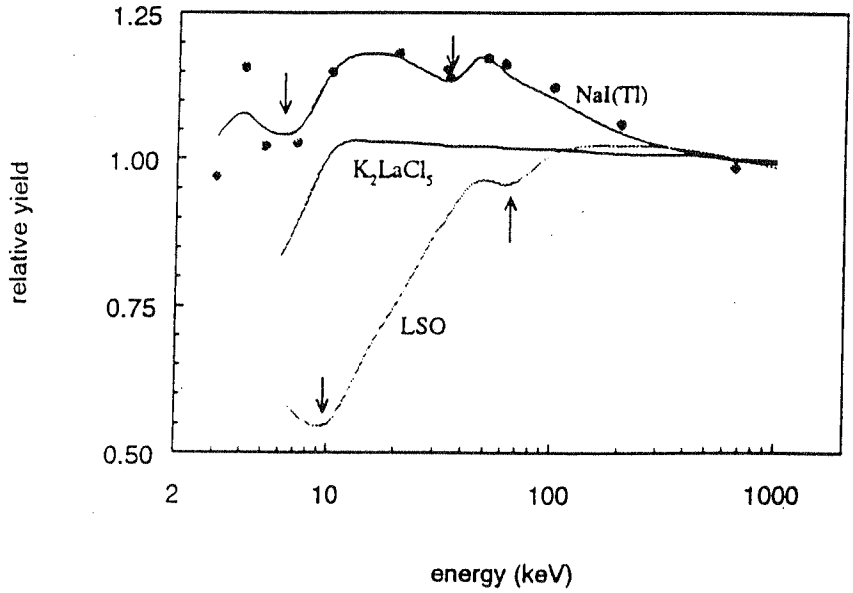

Figure 1: Response curves of $NaI(Tl^+)$, $Lu_2SiO_5(Ce^{3+})$(LSO), and $K_2LaCl_5(Ce^{3+})$, normalized to unity at E_γ=662 keV. The experimental data points, not shown in the Figure, for $NaI(Tl^+)$ can be found in [3]. For $K_2LaCl_5(Ce^{3+})$ and $Lu_2SiO_5(Ce^{3+})$ see [5]. The data points are results from Monte Carlo simulations of the scintillation process in $NaI(Tl^+)$. The arrows show the position of K-shell and L-shell binding energies.

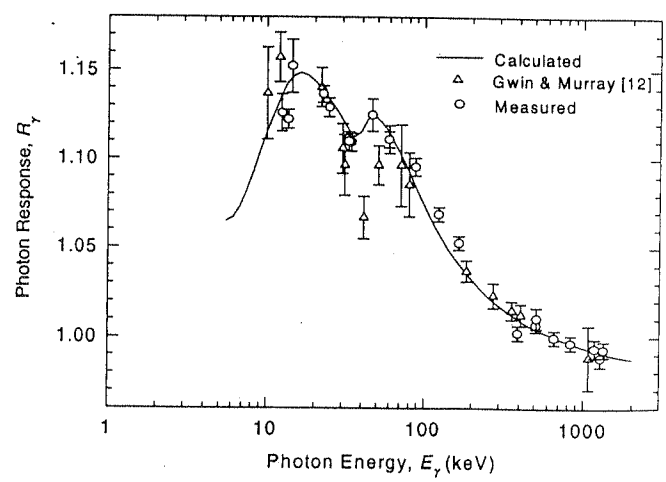

Figure 4: CsI(Tl) calculated and measured photon responses $R_\gamma(=L_\gamma/E_\gamma)$. Results from Gwin and Murray [12] have also been included. Data are normalized to unity at 661.66 keV.

Compton scattering

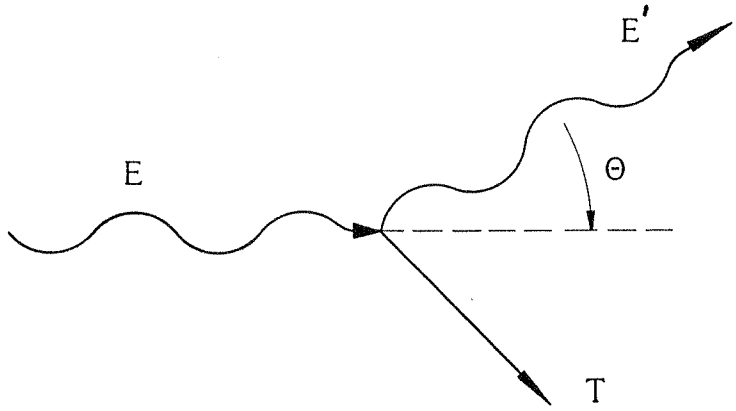

$$E' = \frac{E}{1 + (1 - \cos\theta)\frac{E}{0.511}}$$

$$T = \frac{E^2(1 - \cos\theta)}{E(1 - \cos\theta) + 0.511}$$

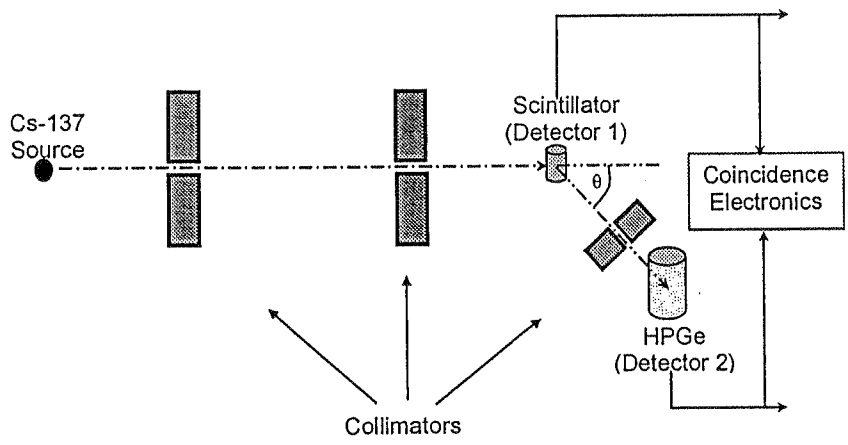

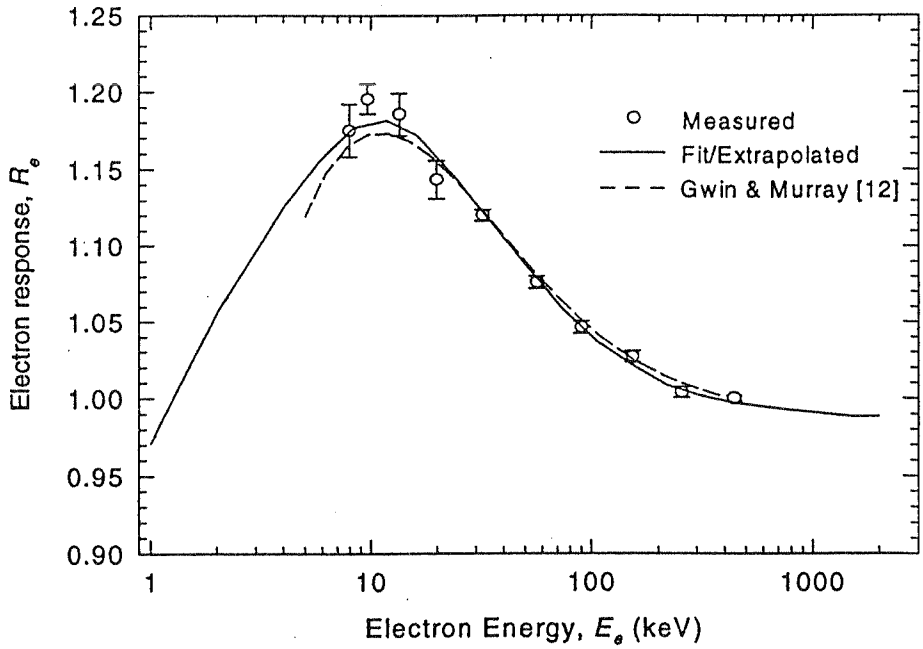

Figure 3: CsI(Tl) electron response $R_e(=L/E_e)$ measured using the CCT along with a smooth fit and low and high energy extrapolations used in photon response calculations. Also shown are previously reported calculated results from Gwin and Murray [12]. Data are normalized to unity at 442 keV.

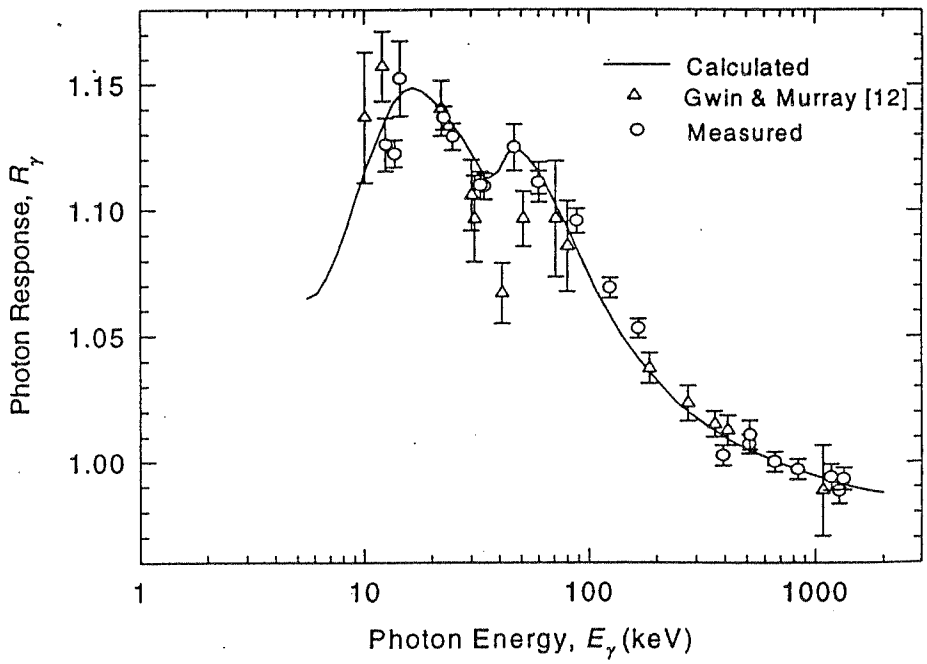

Figure 4: CsI(Tl) calculated and measured photon responses $R_\gamma(=L_\gamma/E_\gamma)$. Results from Gwin and Murray [12] have also been included. Data are normalized to unity at 661.66 keV.

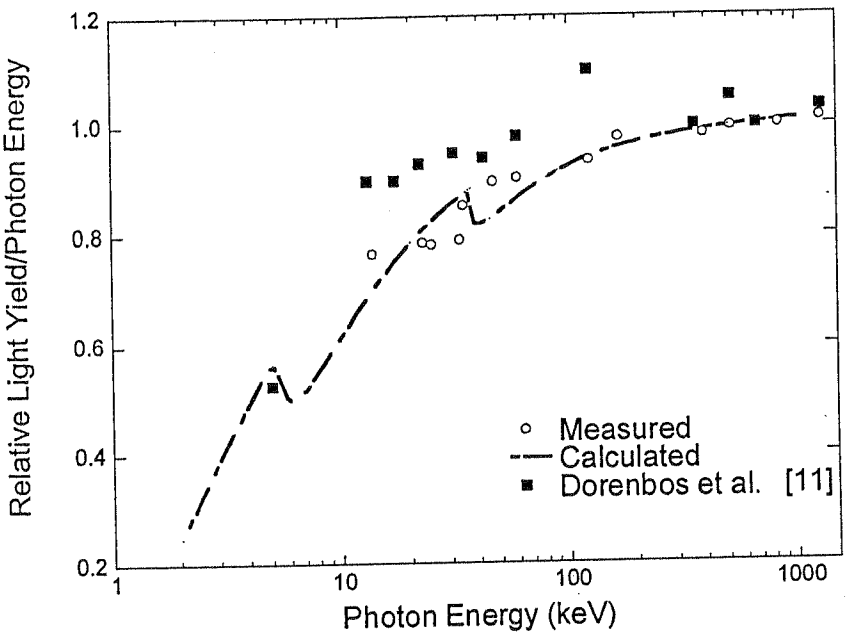

Fig. 5. BaF_2 calculated and measured photon responses. A smooth line is drawn through the calculated response to guide the eye.

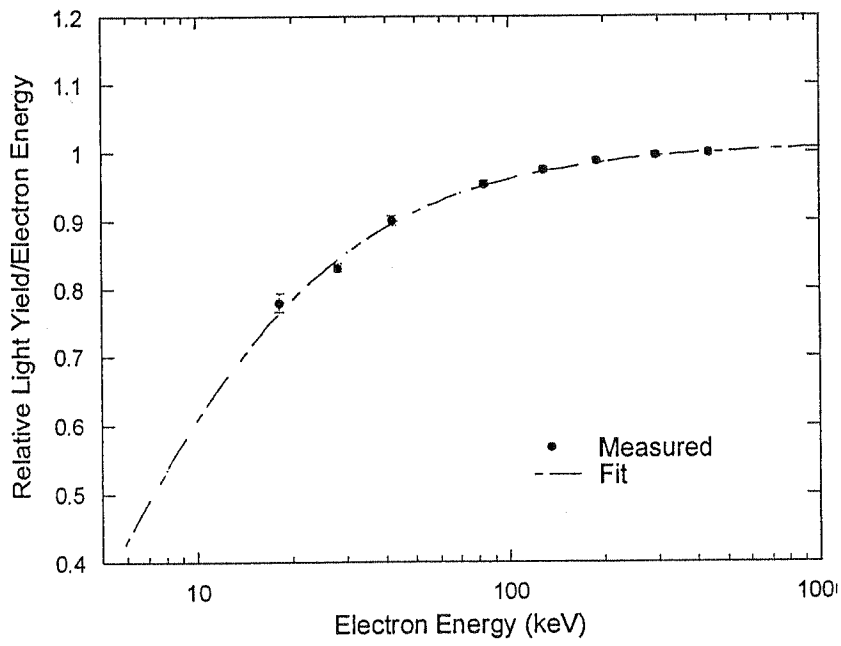

Fig. 4. BaF_2 measured electron response. The response increases by 22% as the electron energy increased from 18 keV to 436 keV.

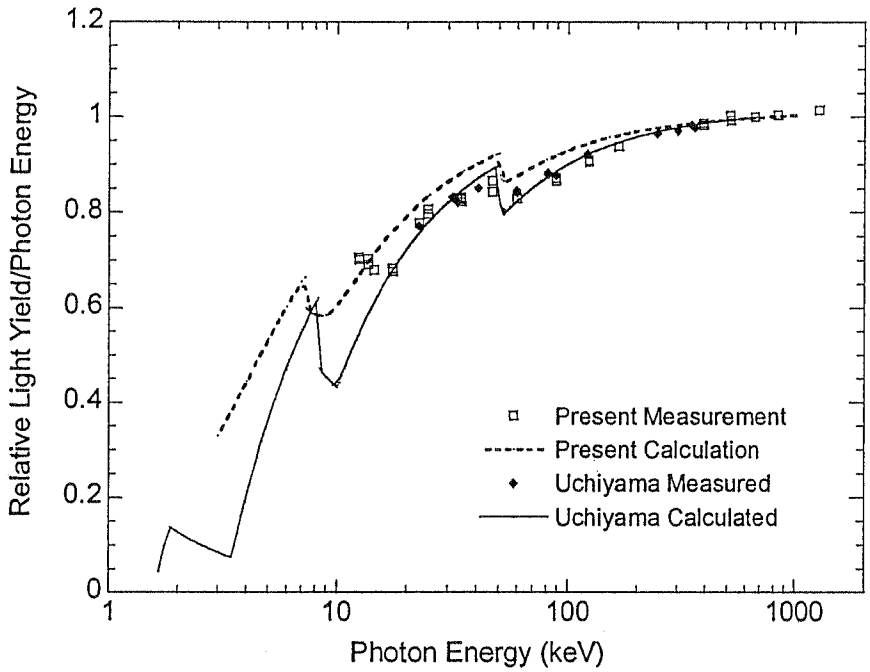

Fig. 3. GSO calculated and measured photon responses. A smooth line is drawn through the calculated response to guide the eye.

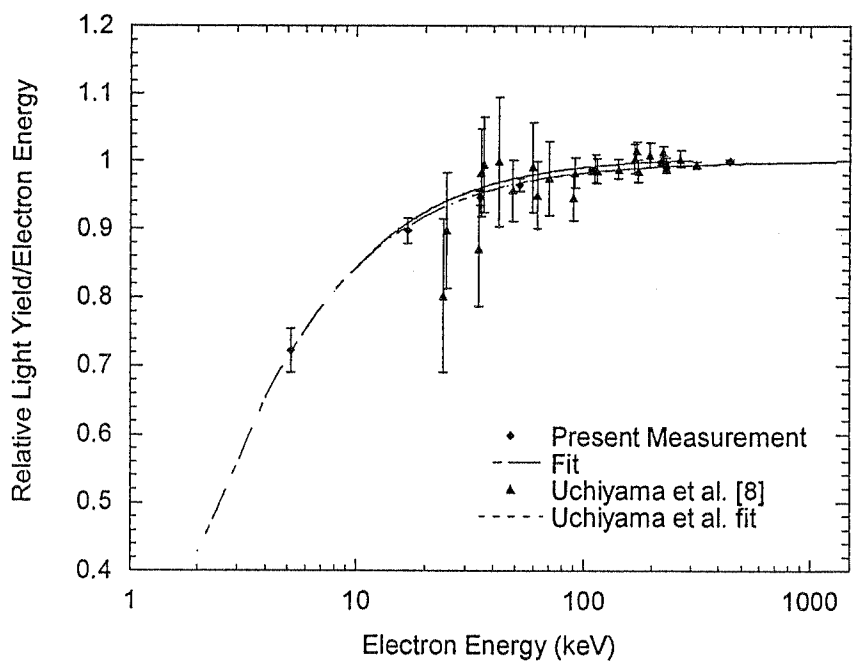

Fig. 2. GSO measured electron response. The response increases by nearly 28% as the electron energy increased from 5 keV to 445 keV.

YSO	$Y_2SiO_5:Ce$
GSO	$Gd_2SiO_5:Ce$
LSO	$Lu_2SiO_5:Ce$
LGSO	$Lu_{1-x}Gd_xSiO_5:Ce$

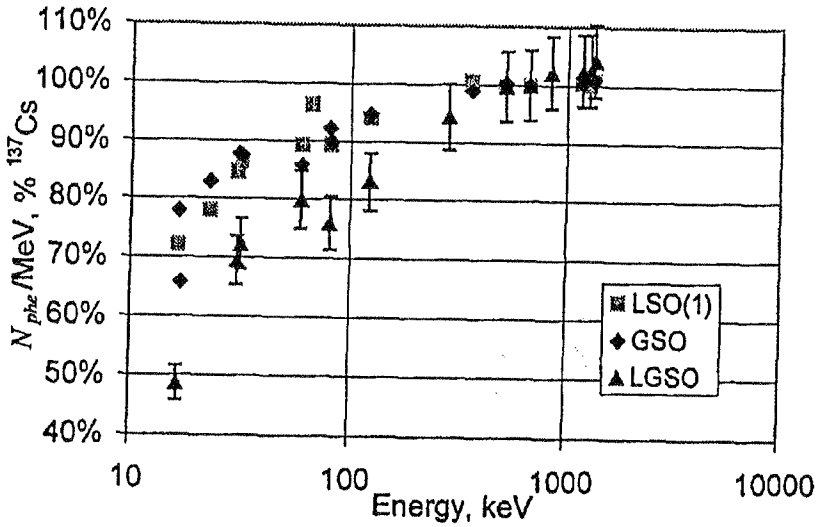

Figure 5. Nonproportionality of the light output for LSO, GSO and LGSO.

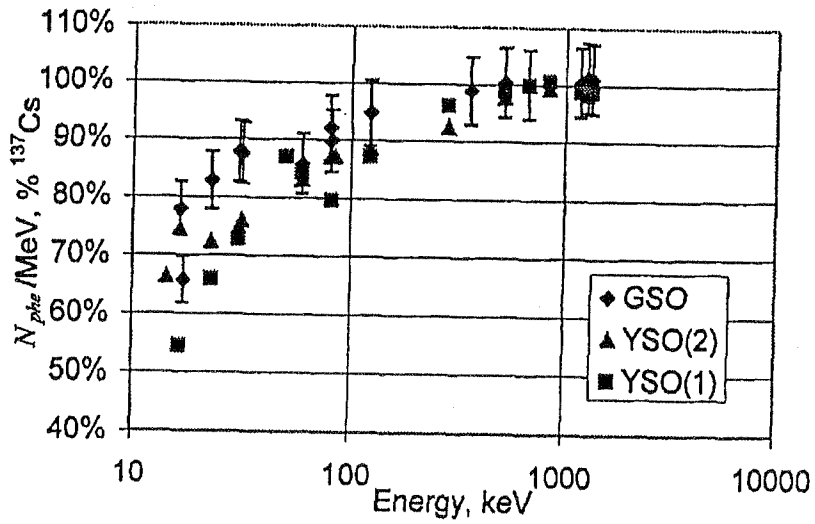

Figure 6. Nonproportionality of the light output for GSO and YSO (1) and (2).

Requirements for new scintillation detectors

- high light yield
- good energy resolution
- fast
- high stopping power
- good mechanical and optical properties

Ways to improve the scintillators

- same crystal but with new dopants
- cooled scintillators
- new materials

	τ [ns]	λ_{max} [nm]	light yield [photons/MeV]
CsI pure	16	315	2 000
CsI(Tl)	800/6000	540	60 000
CsI(Na)	630	420	37 000
CsI(CO_3)	2000	405	26 000

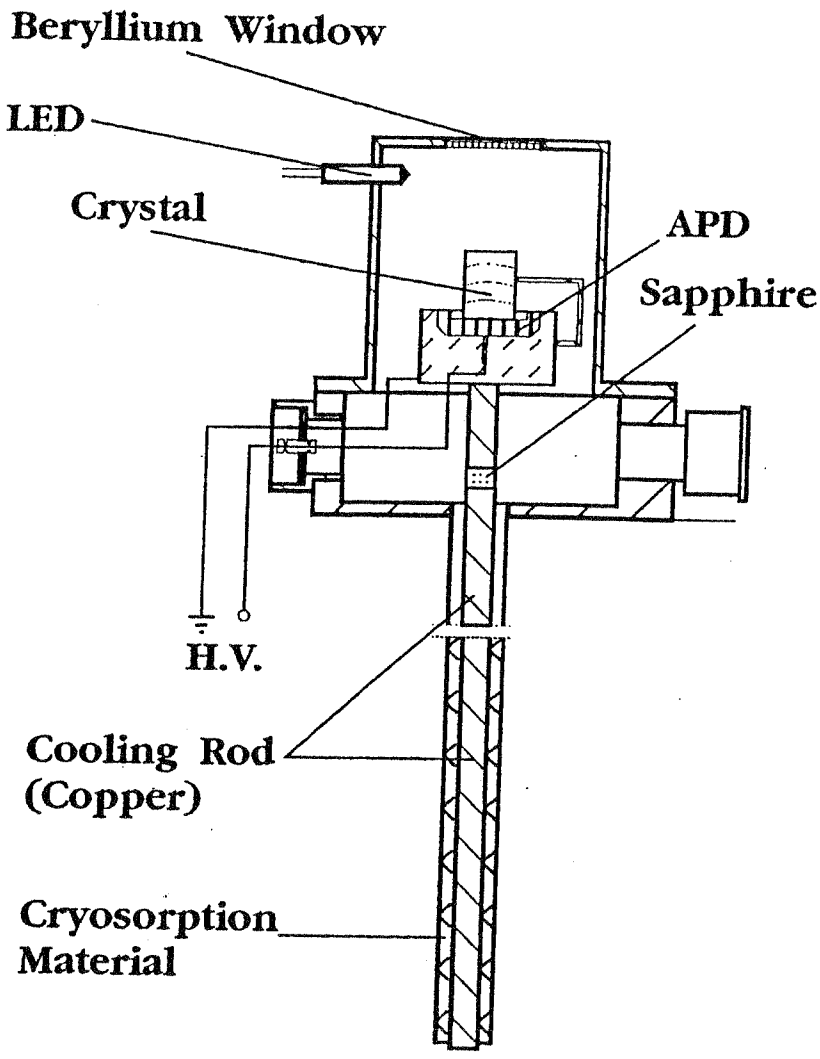

Fig. 1. Schematic drawing of the cryostat with the NaI crystal coupled to the LAAPD.

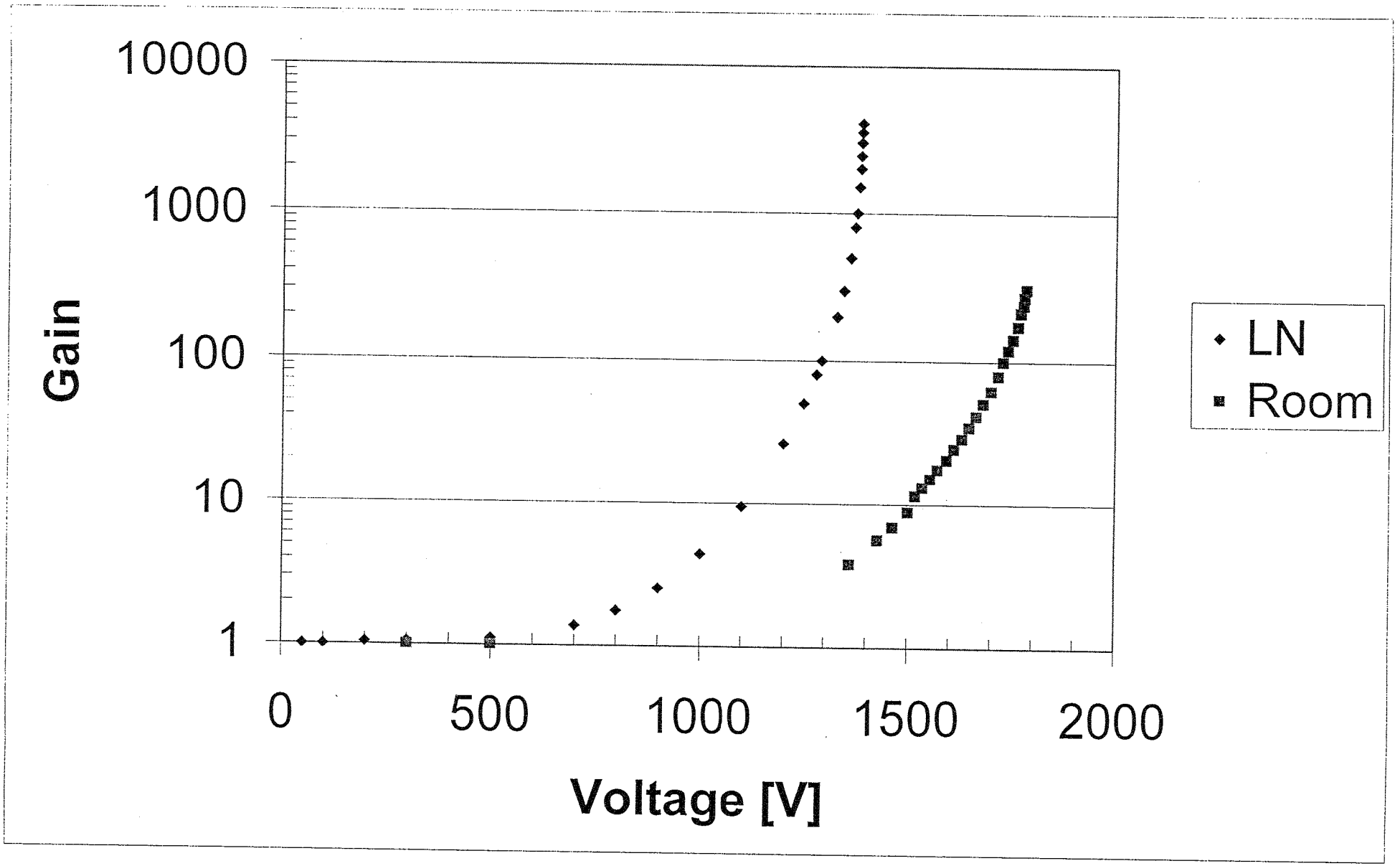
10000
1000
100
10
1
Gain
0
500
1000
1500
2000
Voltage [V]
LN
Room

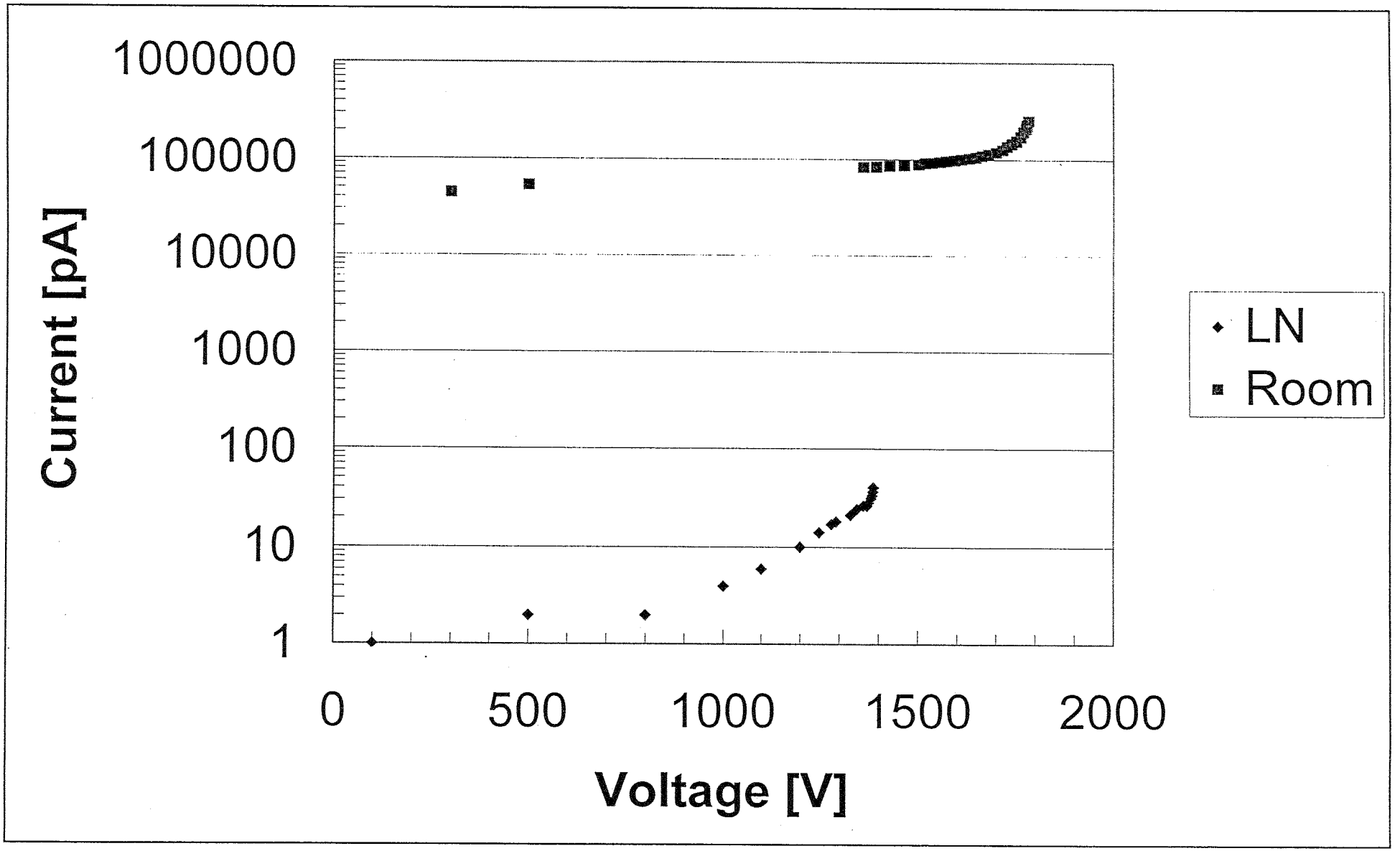
1000000
100000
10000
1000
100
10
1
Current [pA]
0
500
1000
1500
2000
Voltage [V]
LN
Room

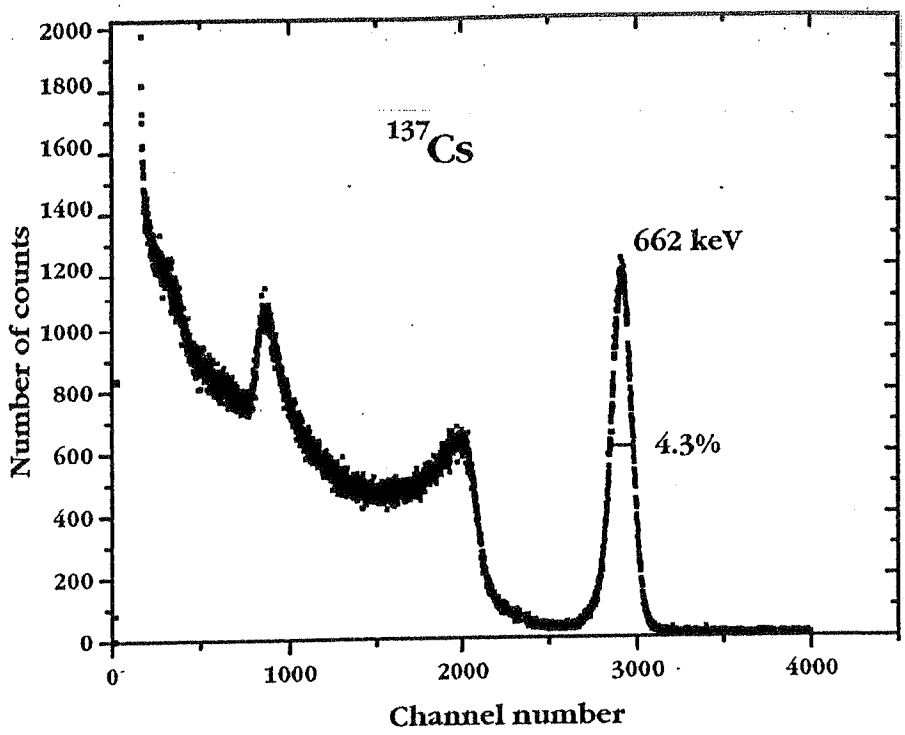

Fig. 6. Energy spectrum of γ-rays from a ^{137}Cs source, as measured with the NaI (B) at LN_2 temperature.

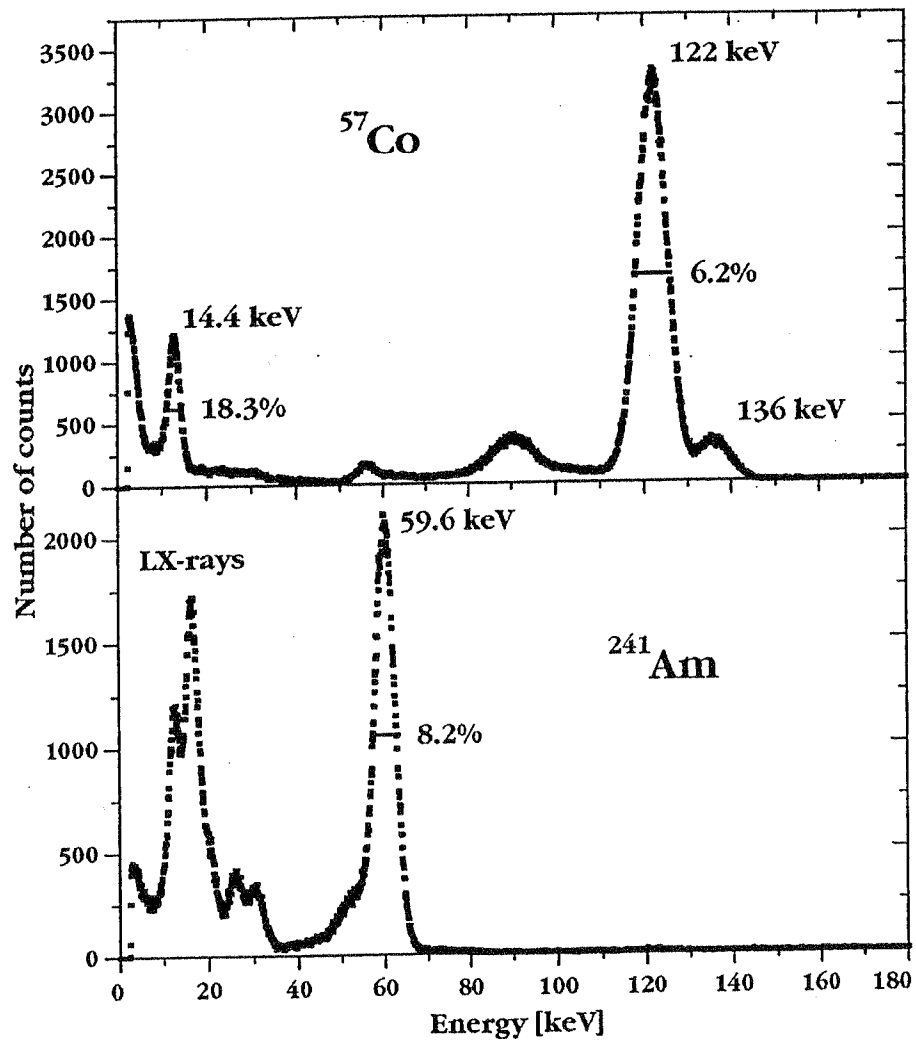

Fig. 7. Energy spectra of γ-rays from ^{241}Am and ^{57}Co sources measured with the NaI (B) at LN_2 temperature.

Pure NaI

	room temp.		*LN_2 temp.*	
crystal	energy resolution (%)	light yield (ph/MeV)	energy resolution (%)	light yield (ph/MeV)
A	16.2±1	4000±400	3.8±0.1	69000±7000
B	16.5±1	3800±400	4.3±0.2	84000±9000
C	14.9±1	2500±250	6.2±0.2	62000±7000

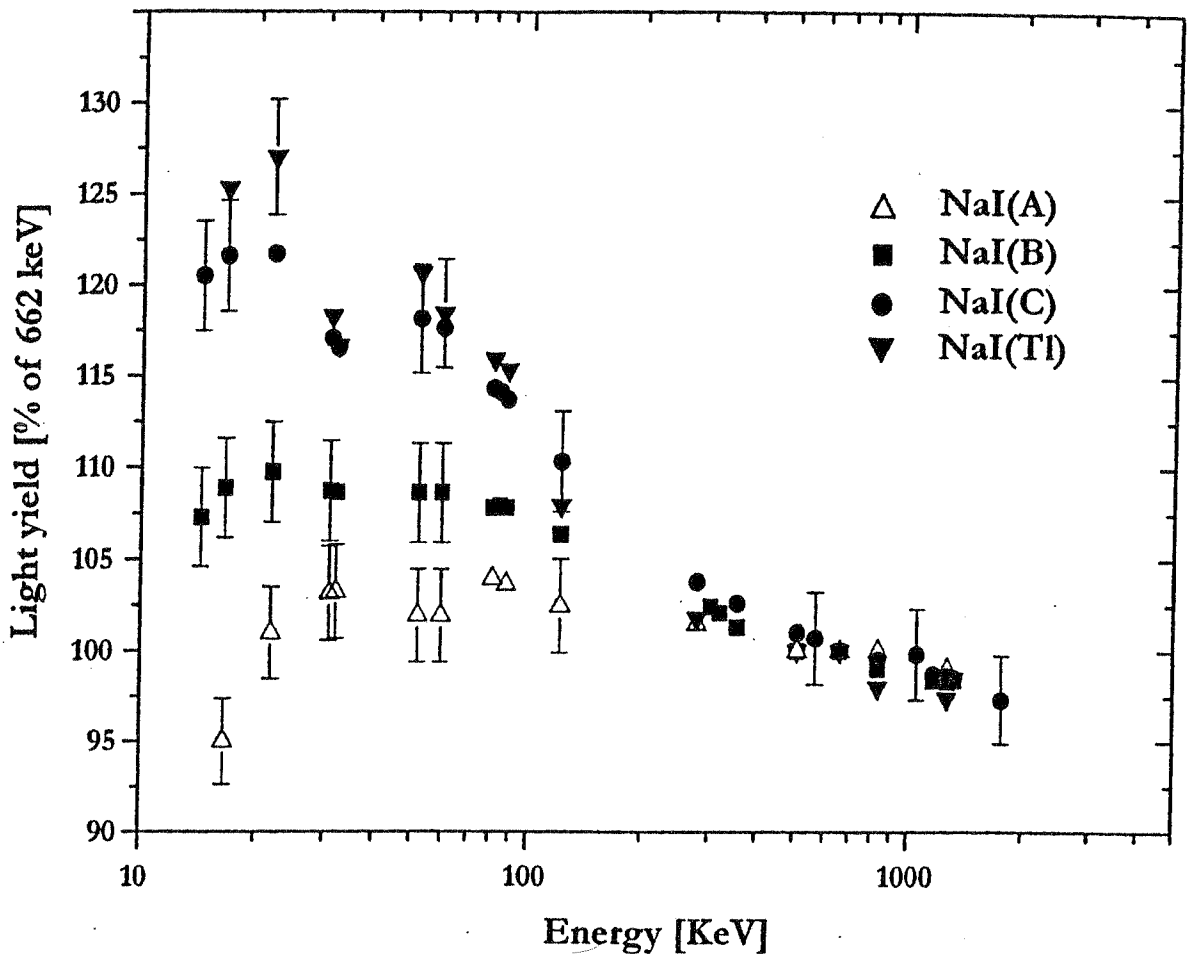

Fig. 8. The non-proportionality curves of studied NaI crystals in comparison to the curve measured for NaI(Tl) coupled to the XP2020Q photomultiplier. Error bars are shown for some selected points.

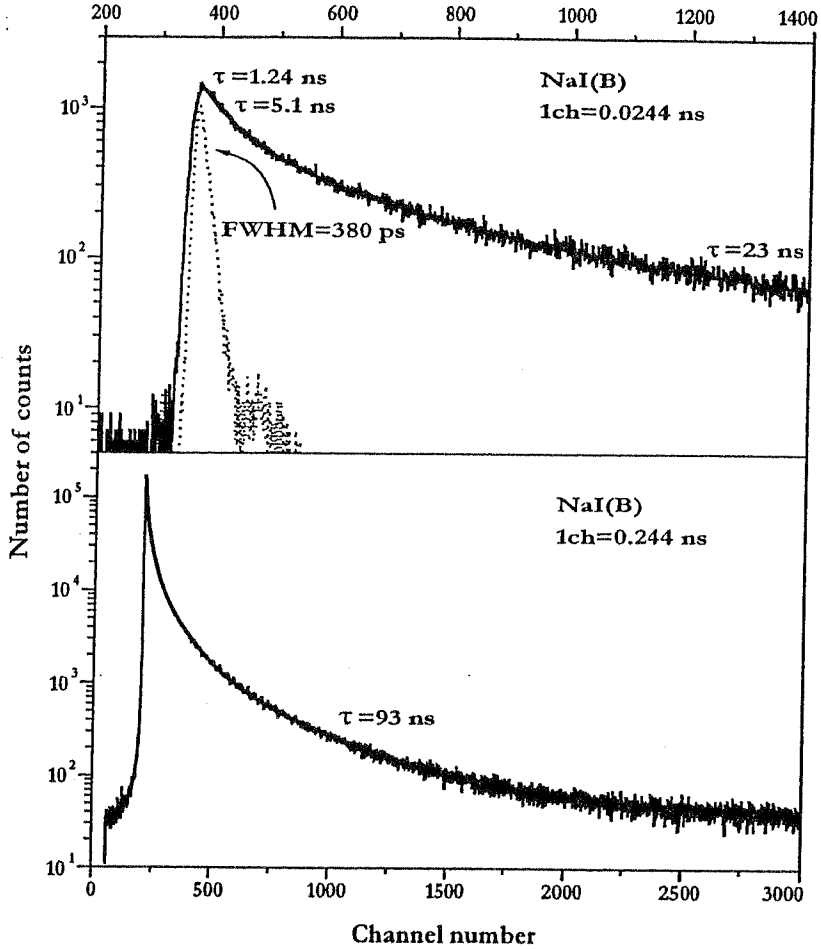

Fig. 4. Light pulse shape from a pure NaI measured at room temperature is shown in two different time intervals. The prompt spectrum of the timing system is shown in the upper plot.

TABLE II
LIGHT PULSE COMPONENTS OF PURE NaI AT ROOM TEMPERATURE

Crystal	Decay time constants/ intensities			
A	0.86±0.04 ns /7.3±0.4%	4.5±0.1 ns /27.4±0.9%	22.3±0.3 ns /51.5±1.7%	120±3 ns /13.8±0.8%
B	1.24±0.05ns /11.1±0.7%	5.1±0.2 ns /27.6±2.4%	23±1 ns /44.4±4.1%	93±1 ns /16.9±0.3%
C	1.02±0.03 ns /15.2±0.5%	4.2±0.1 ns /30.1±0.9%	18.6±0.3 ns /46.9±1.4%	138±8 ns /7.8±0.6%

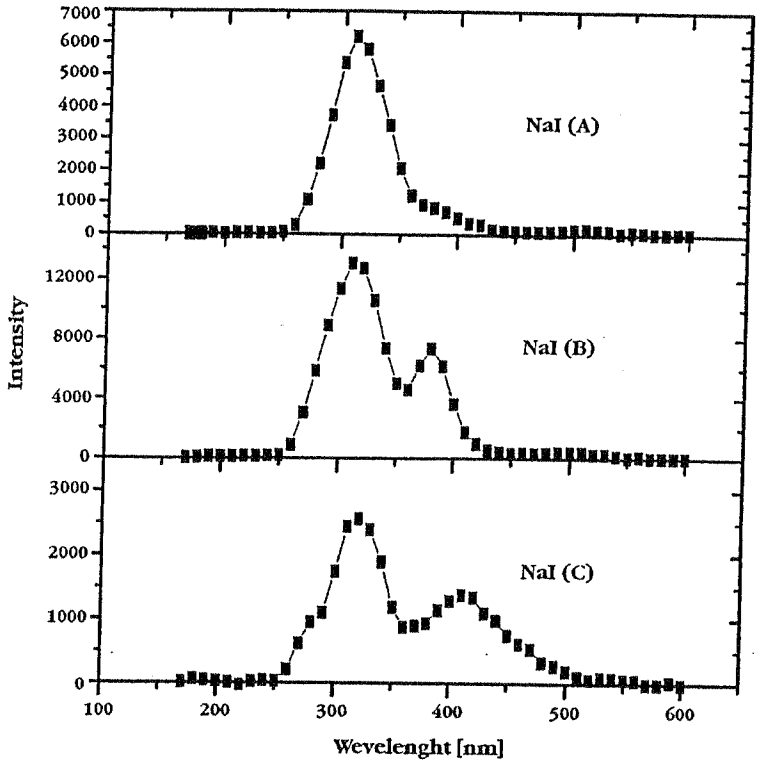

Fig. 2. Emission spectra of tested samples of pure NaI crystal.

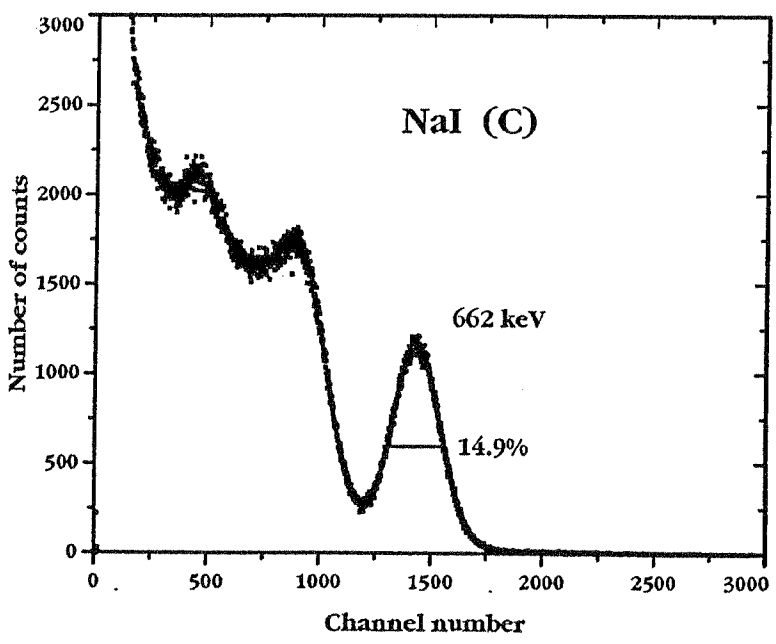

Fig. 3. Energy spectrum of a ^{137}Cs source, as measured with NaI (C).

Room temp.

	τ_d [ns]	λ_{max} [nm]	light yield [ph/MeV]
CsI(Tl)	800/6000	540	60 000
CsI pure	16	315	2 000

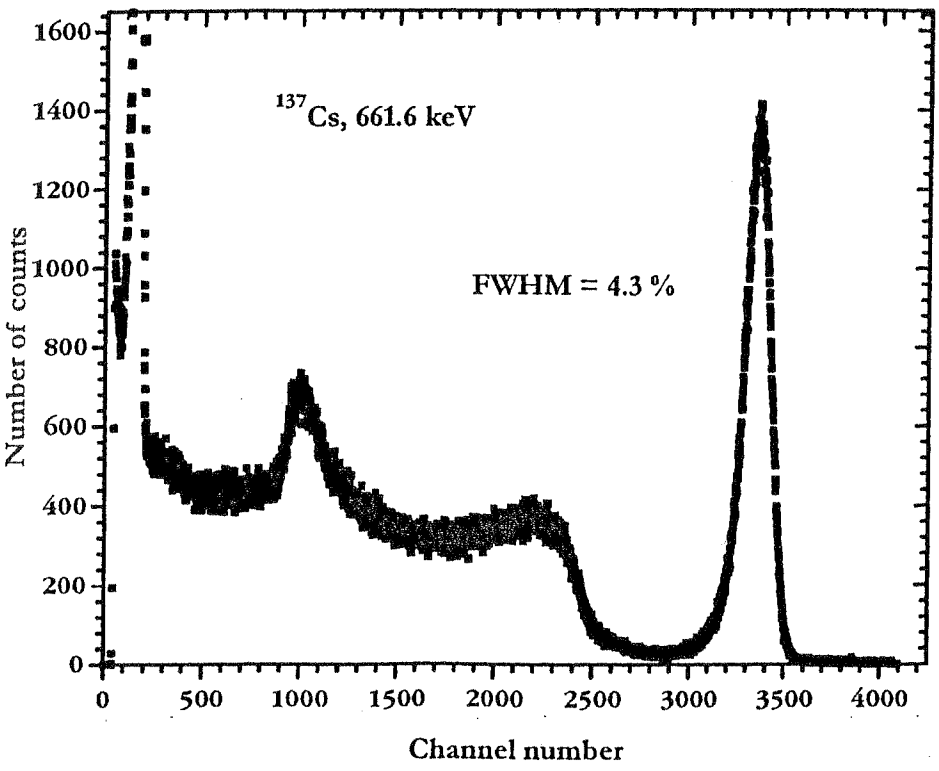

Fig. 2. Energy spectrum of 662 keV γ-rays from a ^{137}Cs source measured with CsI (B).

Table 1

Number of e-h pairs, light output and energy resolution of CsI crystals measured at 662 keV γ-rays

Crystal	$N_{e\text{-}h}$/MeV	ΔE/E [%]	Light output [ph/MeV]
CsI – A	37600±800	5.0±0.2%	108000±10000
CsI – B	43000±900	4.3±0.1%	124000±12000

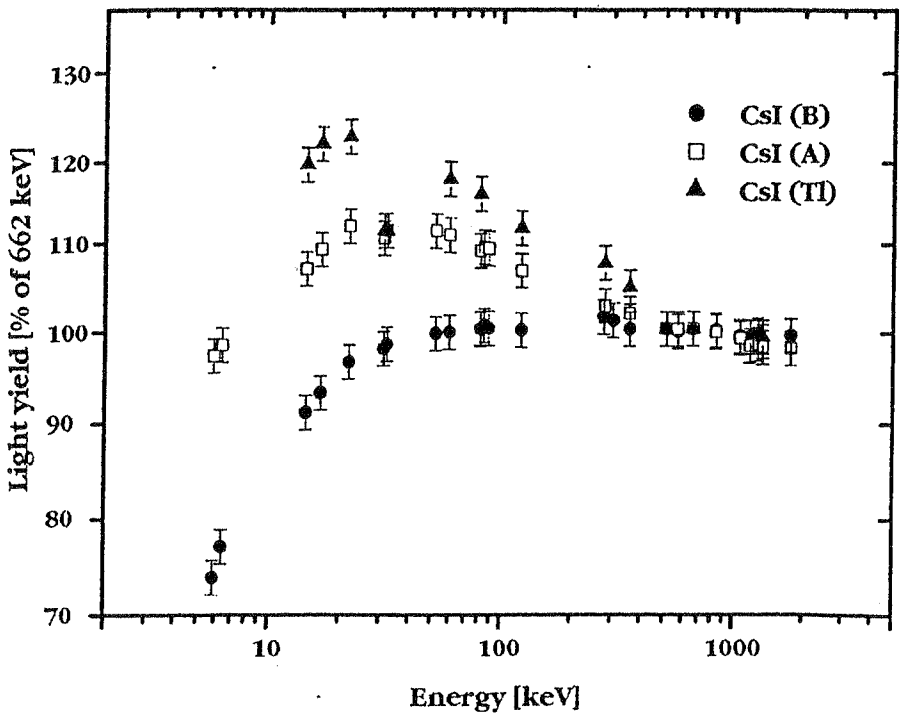

Fig. 3. The non-proportionality curves of studied CsI crystals at LN_2 temperature in comparison to the curve measured for CsI(Tl) coupled to the XP2020Q photomultiplier at room temperature.

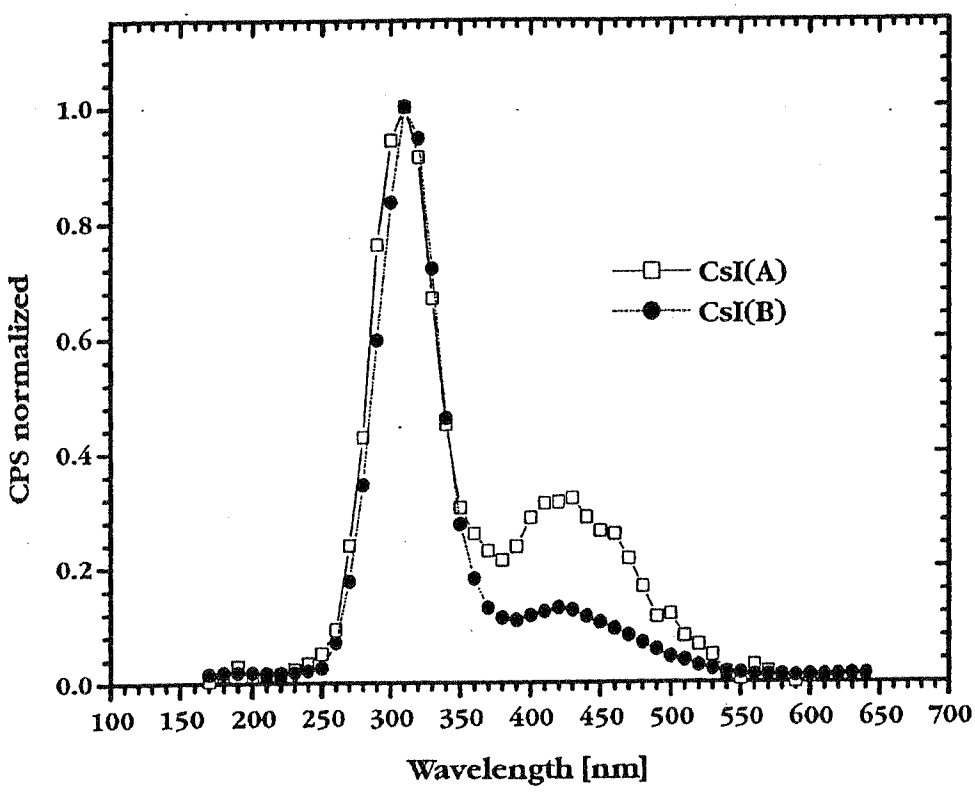

Fig. 8. Emission spectra of tested pure CsI crystals, as measured at room temperature.

BGO ($Bi_4Ge_3O_{12}$)

Crystals diam. 9x4 mm

	room temp.		*LN_2 temp.*	
crystal	energy resolution (%)	light yield (ph/MeV)	energy resolution (%)	light yield (ph/MeV)
BGO 1	10.0±0.3	6900±140	6.5±0.2	29000±2000
BGO 2			6.3±0.2	29500±2000

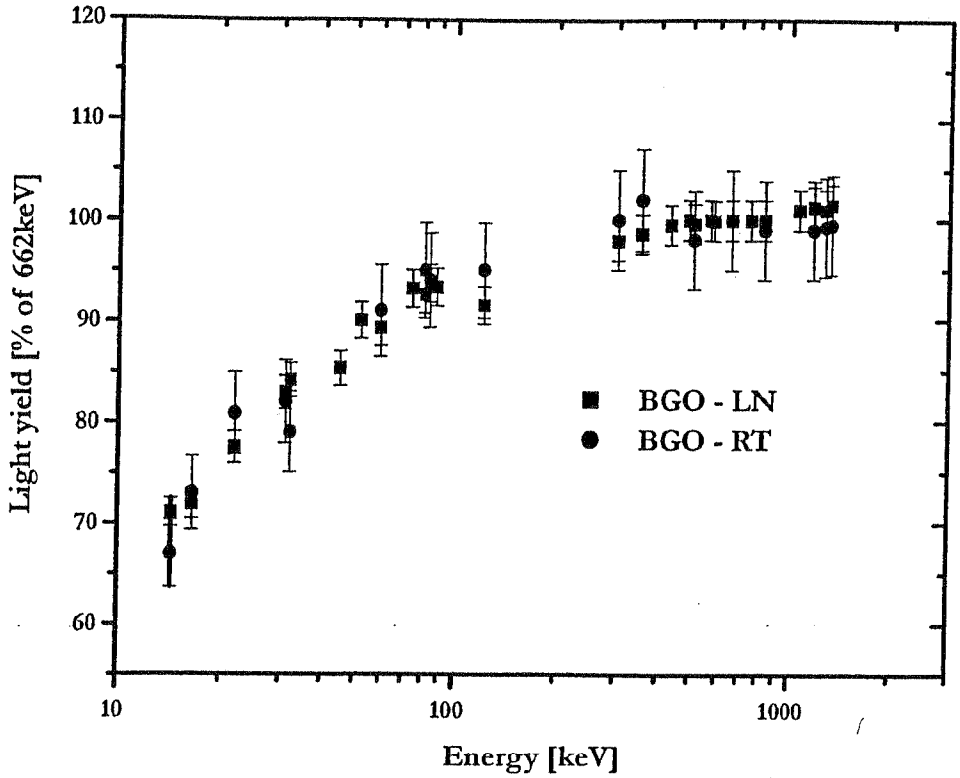

Fig. 6. The non-proportionality characteristics of BGO crystals determined at both room and LN_2 temperatures.

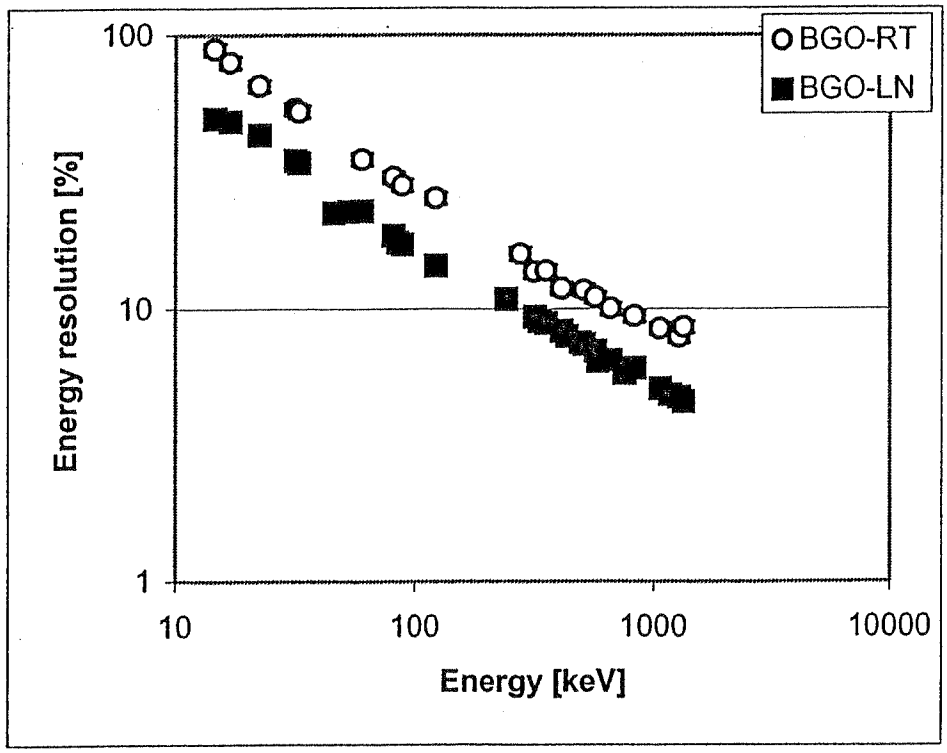

Fig. 7. Energy resolution measured with BGO at room and LN_2 temperature versus energy of gamma rays.

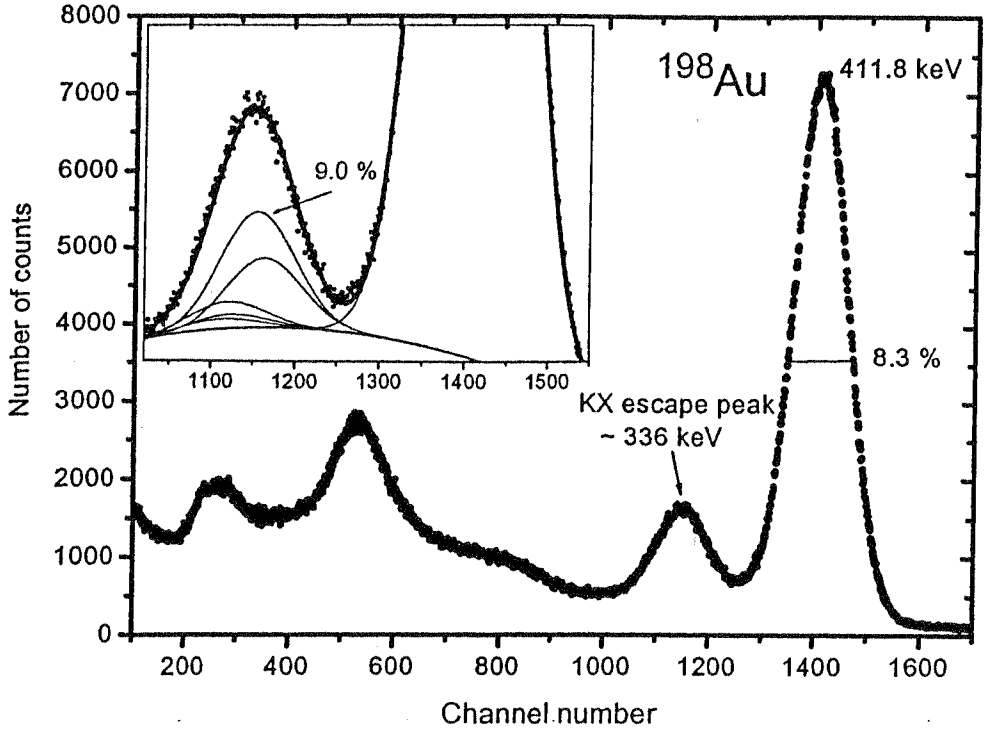
198Au
411.8 keV
9.0 %
8.3 %
KX escape peak
~ 336 keV
Number of counts
Channel number

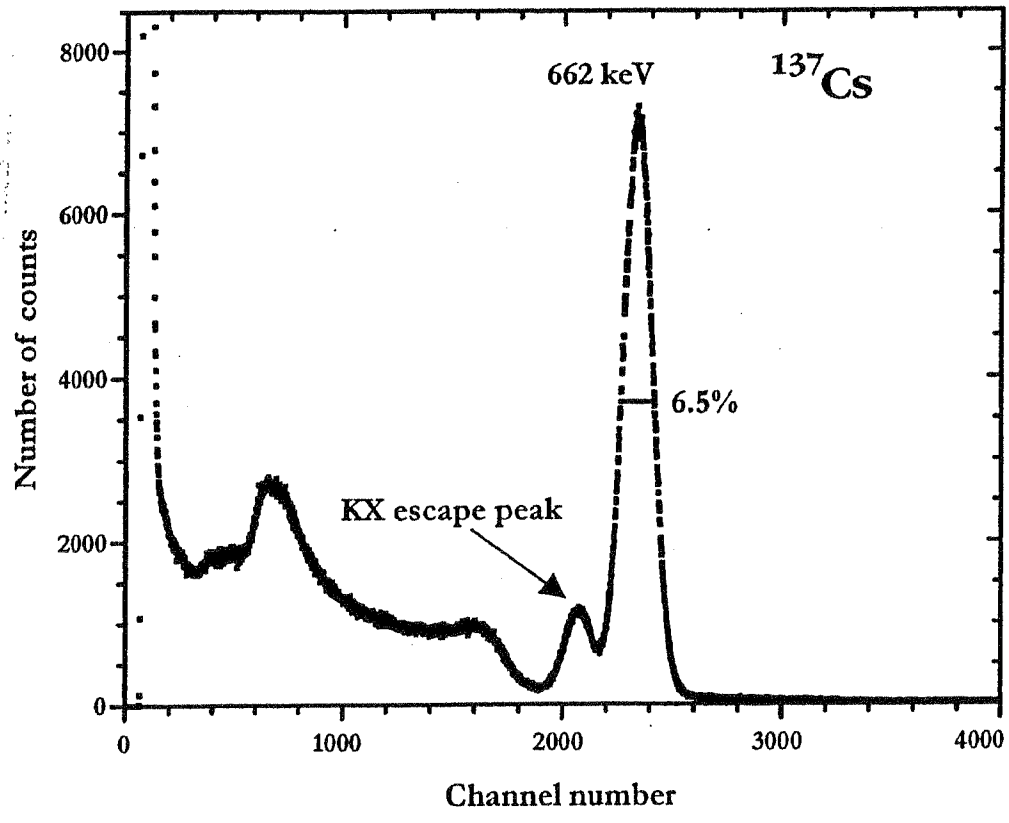
662 keV
137Cs
6.5%
KX escape peak
Number of counts
Channel number

$LaBr_3$:Ce
(0.5 % Ce)

density: 5.29 g/cm^3
hygroscopic
λ_{max}=358 nm
τ= 35 ns
light output: 61 000 ph/MeV

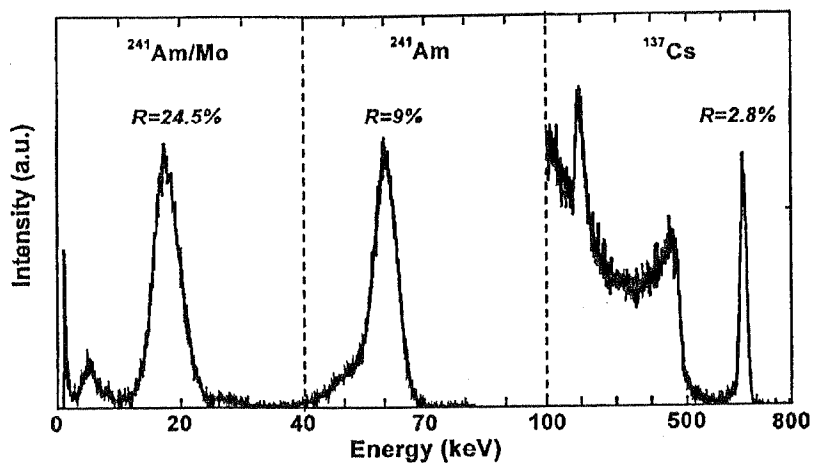

FIG. 1. Energy resolution obtained with a single crystal of $LaBr_3$:0.5% Ce^{3+} for x/γ rays from ^{137}Cs, ^{241}Am, and ^{241}Am/Mo source.

$LaCl_3$:Ce

density: 3.86 g/cm^3
hygroscopic

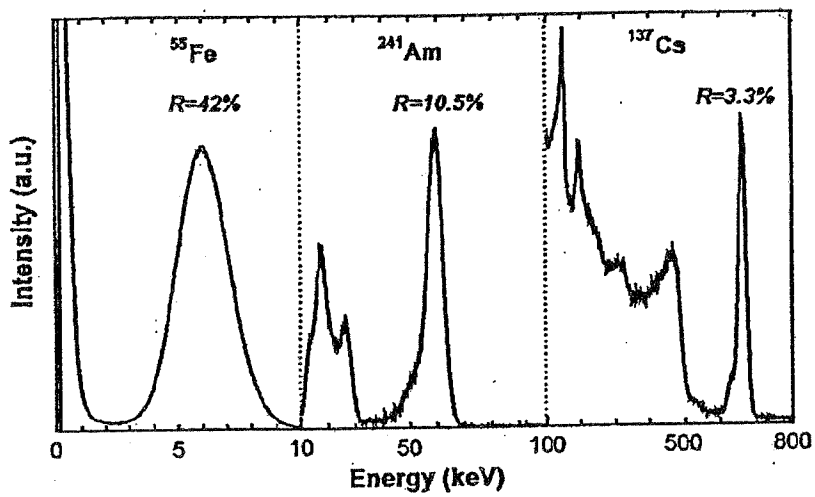

FIG. 1. Energy resolutions obtained with a single crystal of $LaCl_3$:Ce 10% for x/γ rays from (a) ^{55}Fe, (b) ^{241}Am, and (c) ^{137}Cs sources.

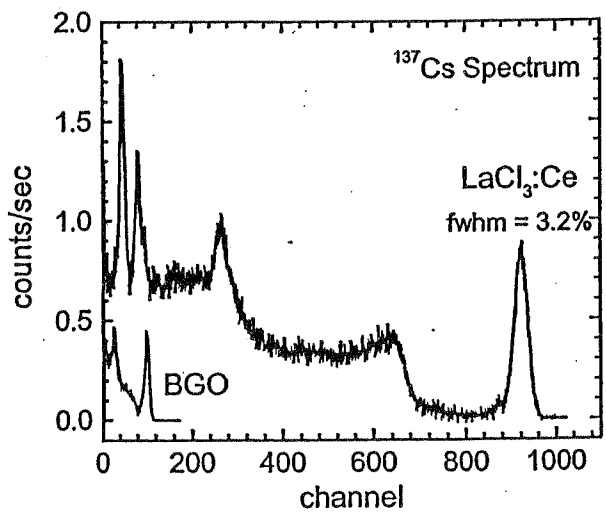

Fig. 1. ^{137}Cs spectra recorded with $LaCl_3$:10% Ce and BGO crystals coupled to PMT under identical operating conditions. Light output of $LaCl_3$:10% Ce was estimated to be ~50,000 photons/MeV from the calibration provided by BGO. The $LaCl_3$ spectrum shows resolution of 3.2% (FWHM) at room temperature.

$LaCl_3$:Ce

% Ce	L.Y [photons/MeV]	τ [ns]	λ [nm]
0.1	50 500	20 (15%), 213 (85%)	350, 430
1	50 500	20 (33%), 213 (67%)	350, 430
10	50 000	20 (70%), 213 (30%)	350, 430
20	38 000	25 (76%), 63 (13%), 213 (11%)	350, 430

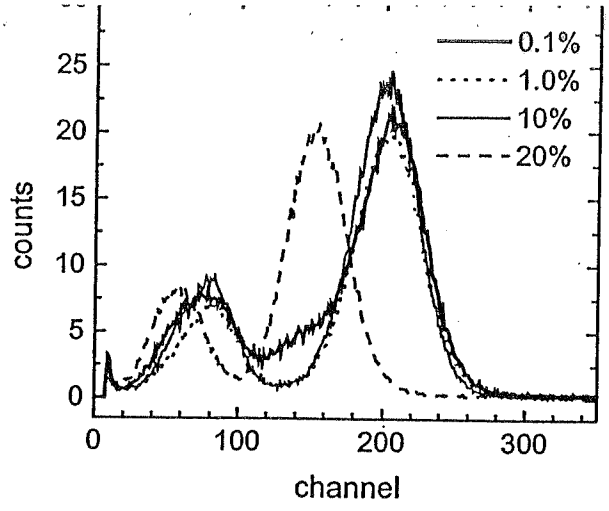

Fig. 2. ^{241}Am spectra (60 keV photons) recorded with $LaCl_3$:Ce crystals of different Ce concentrations. From the peak position light output was estimated for each crystal, see Table 1.

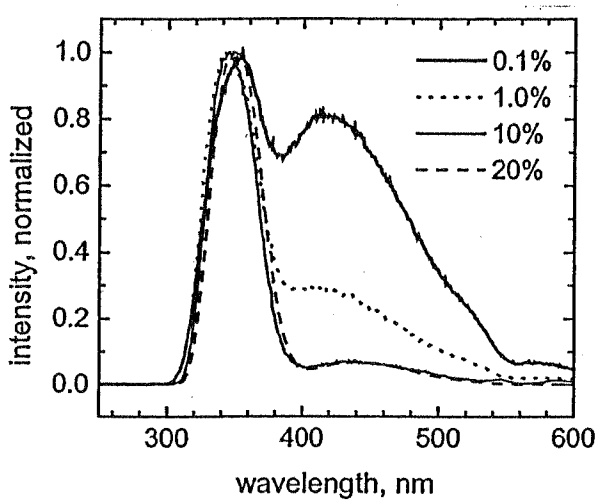

Fig. 3. Optical emission spectra for $LaCl_3$ samples with different Ce concentrations. Spectra were normalized with respect to 350 nm peak intensity.

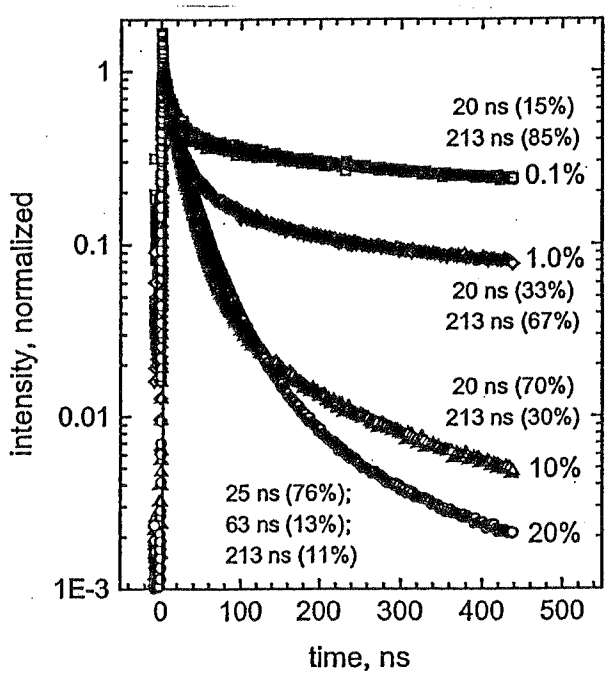

Fig. 4. Time profiles (points) measured for $LaCl_3$ crystals with 0.1%, 1.0%, 10%, and 20% Ce concentrations, along with multi-exponential fits (lines). As seen in plots, the principal decay constant is fast ($\leqslant$25 ns) for samples with high (10–20%) Ce concentration.

LYSO

$LuYSiO_5$:Ce

density: 7.1 g/cm^3

λ_{max}=430 nm

τ= 48 ns

light output: 32 000 photons/MeV

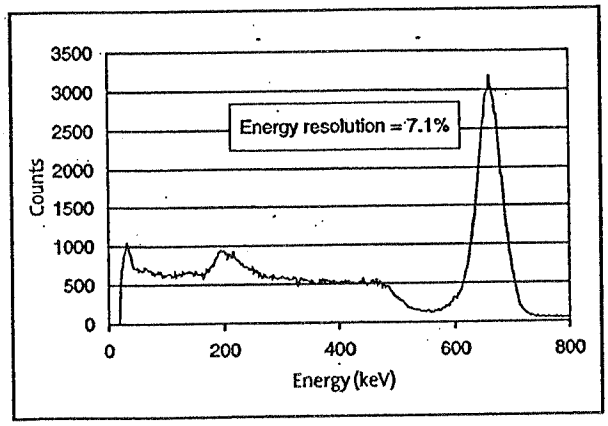

Figure 1. LYSO Response to 662 keV Photons

	L.Y [ph/MeV]	energy resolution [%]	time resolution [ps]
$LaBr_3$:Ce	61 000	2.8	385
$LaCl_3$:Ce	50 000	3.2	224
LYSO:Ce	32 000	7.1	-